Finite element model updating of a geared rotor system using particle swarm optimization for condition monitoring

Morteza Farrokhnia, Farzad A. Shirazi[*], Maryam Mahnama, Mohammad Mahjoob

School of Mechanical Engineering, College of Engineering, University of Tehran, Tehran, Iran

A B S T R A C T

In this paper, condition monitoring of a geared rotor system using finite element (FE) model updating and particle swarm optimization (PSO) method is considered. For this purpose, employing experimental data from the geared rotor system, an updated FE model is obtained. The geared rotor system under study consists of two shafts, four bearings, and two gears. To get the experimental data, piezoelectric accelerometers are mounted on the bearings to extract the natural frequencies. Also, mass, stiffness and gyroscopic matrices can be obtained using FE method. By extracting these matrices, natural frequencies and mode shapes are also obtained from solutions of an eigenvalue problem. Having the first flexural four natural frequencies from experimental modal analysis as the objective, FE model of the geared rotor structure is to be updated. Solving sensitivity equations iteratively, model updating is performed to predict the required changes in parameters of the model. In the next stage, some defects are introduced into the experimental setup and the resulting natural frequencies are set as the reference for model updating purpose. Therefore, the changes in the model parameter with respect to a healthy system is monitored. Using PSO method, fault detection in a geared rotor system is performed. Model updating and PSO are able to predict the types and values of damages created in the geared rotor system. In general, the model updating method is simpler and computationally more efficient for industrial equipment. However, particle swarm optimization provides more accurate results with higher computations.

© 2019 Iranian Society of Acoustics and Vibration, All rights reserved.

[*] Corresponding author.
   E-mail addresses : fshirazi@ut.ac.ir (F. A.Shirazi)

1. Introduction

Gears are widely used in industrial, automotive, and daily-life applications for mechanical power transmission. Depending on the design of the system, gears offer advantages in producing high-speed ratio, changing the torsion direction, and transmitting a high load efficiently. Gear failure is an unwanted event, as it terminates the functionality of the gear and may entail serious and costly consequences.

Therefore, it is important to monitor the health of gearbox systems and detect their faults as early as possible. Early detection allows proper scheduled shutdown and maintenance to prevent catastrophic failure and consequently guarantees a safer operation and higher cost reduction[1]. There are mainly two types of approaches for gear fault diagnostics: signal-based and physical model-based methods. Signal-based methods purely rely on the analysis of historical data collected from gearboxes to diagnose and/or predict their health condition. The measured data could be vibration signals, torque load signals, acoustic signals, metal scan data, gear weight loss data, gearbox strain signals, and gear damage images. Different signal-based methods have been developed for gearbox fault diagnostics [2-5].

In physical model-based methods, a virtual system is built to mimic an existing object based on human understanding of this object. The physical models of gearboxes can be divided into two subsets: modulation based models and dynamics based models. Modulation based models are developed via the understanding of amplitude modulation and frequency modulation characteristics of vibration signals. The studies on the development of modulation based models are available in [6-8]. Dynamics based models are developed based on a fundamental analysis of a dynamic model of the gear mechanism. Therefore, dynamic characteristics in various health conditions can be simulated. Then the fault symptoms can be revealed and summarized for fault detection and diagnosis. Parey and Tandon [9] reviewed spur gear dynamic models and considered the gear faults such as wear and spalling. Bartelmus [10] considered mathematical modelling and computer simulations for supporting fault detection in gearbox systems. Lei *et al*. [11] reviewed condition monitoring techniques for fault diagnosis of planetary gearboxes. Ma *et al* [12]. reviewed dynamics of cracked gear systems including crack propagation path modelling and dynamic models for vibration analysis of cracked gear systems. Lee *et al*.[13] considered the coupled lateral and torsional vibration characteristics of the rotor-bearing system using finite element model of a gear pair, bearings, and shafts for providing the mechanism of the characteristic changes.

Finite Element (FE) model updating is a procedure aimed at calibrating the FE model of a structure in order to match the experimental results. Introduced in the 1980s, it turned out to play a crucial role in the design, analysis and maintenance of aerospace, mechanical and civil engineering structures[14, 15]. In structural mechanics, model updating techniques are used in conjunction with vibrations measurements to determine unknown system characteristics, such as material properties, constraints, etc. A further important application of model updating, within the field of structural health monitoring, is damage detection [16, 17]. Damage can be identified based on the assumption that its presence is associated with a decrease in the stiffness of some elements, with consequent changes to the structure modal characteristics. Explanation of sensitivity method in the FE model updating is provided by Mottershead *et al*.[18]. An example of model updating of a helicopter airframe is also discussed in the paper.

Particle swarm optimization (PSO) was proposed by Kennedy and Eberhart as a population-based stochastic optimization technique inspired by the social behavior of bird flocking or fish schooling[19]. PSO is an algorithm based on the group (swarm) behavior. The algorithm searches for the optimal value by sharing the cognitive and social information among the individuals (particles) in the global solution space. The popularity of PSO is growing with applications in diverse fields of engineering, biomedical and social sciences [20]. Some of the recent applications of PSO in engineering include machinery condition monitoring and diagnostics [21].

In this paper, condition monitoring of power transmission gears by model updating method and PSO is considered. The research includes two parts: 1) simulating the geared rotor system by FE method to obtain modal characteristics of the system, 2) extracting modal characteristics of the experimental setup by piezoelectric accelerometer. In this part, model updating is applied to achieve the updated model of the structure and then to detect damages in the system. The advantage of model updating and PSO is to detect damages without simulating the fault and it only works by the differences in modal characteristics. Hence, the differences in the first flexural four natural frequencies are considered. The sensitivity method in FE model updating is used. The sensitivity method is based upon linearization of the generally non-linear relationship between the measurable outputs such as natural frequencies, mode shapes, or displacement responses of the model parameters in need of emendation. Also, in PSO method an error function as a difference between the modal data obtained from computer simulation and experiment is defined. The estimated parameters are attained by minimizing the error function with respect to the tuning parameters. Finally, the results of two methods are compared in the final section.

2. Coupled finite element model of a geared rotor system

The configuration of the geared rotor-bearing system is shown in Fig. (1). Two flexible shafts with the gear pair, as two rigid disks, are modelled. The bearings are modelled as flexible elements with known stiffness coefficient.
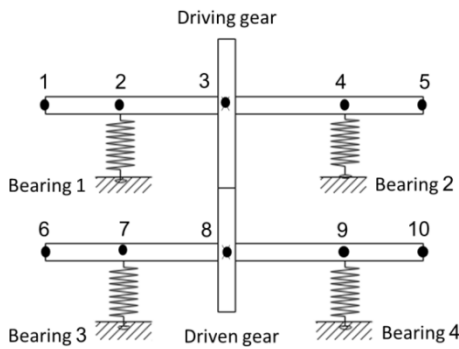
Fig. (1). Geared rotor-bearing system
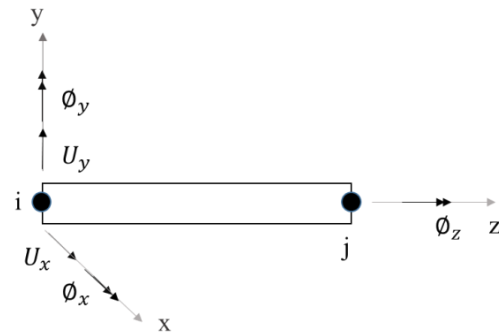
Fig. (2). degrees of freedom of each nodal point

The equations of motion for the system are described in a fixed reference frame xyz. Fig. (2) shows a single shaft system with the rigid disk in y-z plane. Each shaft is divided into four elements and five nodes. At each nodal point of the shaft, five degrees of freedom are considered

in which the U_x and U_y are lateral displacements along x and y directions, respectively. Also ϕ_x and ϕ_y are rotational and ϕ_z is torsional angles about x, y and z axes, respectively.

Neglecting the vibrations along axial direction of the shaft, the flexural and torsional displacement vectors $\{q^e_{fl}\}$ and $\{q^e_{to}\}$ for each rotor element can be defined as:

$$q^e_{fl} = \left\{ U_{xi} \quad U_{yi} \quad \phi_{xi} \quad \phi_{yi} \quad U_{xj} \quad U_{yj} \quad \phi_{xj} \quad \phi_{yj} \right\}^T$$

$$q^e_{to} = \left\{ \phi_{zi} \quad \phi_{zj} \right\}^T \tag{1}$$

The indices i and j indicate the beginning and the end of the element (e). The components of the system include the gear pair, bearing supports and rotor shafts whose equations of motion are introduced in the following section.

2.1. Finite element model of the rotor

In this section, equations of motion for elements are developed by Lagrange's equation. Rotor elements are considered as Euler-Bernoulli beams. The flexural potential energy of the rotor element at the position "s" can be calculated from [7]:

$$dU_e = \frac{1}{2} EI_a \{q^e_{fl}\}^T \left[\psi''_{fl} \right]^T \left[\psi''_{fl} \right] \{q^e_{fl}\} ds \tag{2}$$

where E represents Young's modulus, I_a is the moment of inertia of the beam about the x-axis and $[\psi''_{fl}]$ is the second derivative of the flexural shape function matrix $[\psi_{fl}]$ corresponding to the eight translational and rotational degrees-of-freedom beam element $\{q^e_{fl}\}$. The flexural shape function matrix for the element with the length $"l"$ at the position "s" is shown.

$$[\psi_{fl}] = \begin{bmatrix} \psi_1 & 0 & 0 & \psi_2 & \psi_3 & 0 & 0 & \psi_4 \\ 0 & \psi_1 & -\psi_2 & 0 & 0 & \psi_3 & -\psi_4 & 0 \end{bmatrix}$$

$$\psi_1 = 1 - 3(\frac{s}{l})^2 + 2(\frac{s}{l})^3 \qquad \psi_2 = s\left[1 - 2(\frac{s}{l}) + (\frac{s}{l})^2 \right] \tag{3}$$

$$\psi_3 = 3(\frac{s}{l})^2 - 2(\frac{s}{l})^3 \qquad \psi_4 = l\left[-(\frac{s}{l})^2 + (\frac{s}{l})^3 \right]$$

Also, the rotational shape function matrix is calculated. $\psi'_1, \psi'_2, \psi'_3$ and ψ'_4 are the derivative of translational shape function matrix with respect to "s".

$$[\psi_{ro}] = \begin{bmatrix} 0 & -\psi'_1 & \psi'_2 & 0 & 0 & -\psi'_3 & \psi'_4 & 0 \\ \psi'_1 & 0 & 0 & \psi'_2 & \psi'_3 & 0 & 0 & \psi'_4 \end{bmatrix} \tag{4}$$

98

The torsional potential energy of the rotor element at the position "s" can also be obtained by[22]:

$$dU_e = \frac{1}{2} G_t \bar{I}_p \{q_{to}^e\}^T [\phi_{to}']^T [\phi_{to}'] \{q_{to}^e\} ds \tag{5}$$

where G_t represents the shear modulus, $\bar{I}_p$ is the polar moment of inertia per unit length of the rotor and $[\phi_{to}']$ is the first derivative of the torsional shape function matrix $[\phi_{to}]$ corresponding to two torsional degrees-of-freedom beam elements $\{q_{to}^e\}$.

$$[\phi_{to}] = \frac{1}{l}\begin{bmatrix} 1 & -1 \\ -1 & 1 \end{bmatrix} \tag{6}$$

The element potential energy of the beam is calculated by integrating over the length $'ds'$ which is the thickness of a sliced disk from the shaft at the position $'s'$ in Eq. (2) and Eq. (3).

$$U_e = \frac{1}{2}\{q^e\}^T [K^e]\{q^e\} \tag{7}$$

$$q^e = \{U_{xi} \quad U_{yi} \quad \phi_{xi} \quad \phi_{yi} \quad \phi_{zi} \quad U_{xj} \quad U_{yj} \quad \phi_{xj} \quad \phi_{yj} \quad \phi_{zj}\}^T$$

where $[K^e]$ is the element stiffness matrix including flexural stiffness matrix $[K_{fl}^e]$ and the torsional stiffness matrix $[K_{to}^e]$.

$$[K_{fl}^e] = \int_0^l EI_a [\psi_{fl}'']^T [\psi_{fl}''] ds$$

$$[K_{to}^e] = \int_0^l G_t \bar{I}_p [\phi_{to}']^T [\phi_{to}'] ds \tag{8}$$

The kinetic energy of the element is computed as the sum of the flexural and torsional kinetic energy. The kinetic energy of the beam with the length l is calculated as follows:

$$T_{fl}^e = \frac{1}{2}\{\dot{q}_{fl}^e\}^T [m_{fl}^e]\{\dot{q}_{fl}^e\} + \frac{1}{2}\omega^2 \bar{I}_p l + \frac{1}{2}\omega\{\dot{q}_{fl}^e\}^T [n^e]\{q_{fl}^e\}$$

$$T_{to}^e = \frac{1}{2}\{\dot{q}_{to}^e\}^T [m_{to}^e]\{\dot{q}_{to}^e\} \tag{9}$$

$$T^e = T_{fl}^e + T_{to}^e$$

Where,

$$\left[m_{fl}^{e} \right] = \left[m_{tr}^{\ e} \right] + \left[m_{ro}^{e} \right]$$

$$\left[m_{to}^{e} \right] = \int_{0}^{l} \rho \bar{I}_{p} \left[\phi_{to} \right]^{T} \left[\phi_{to} \right] ds$$

$$\left[m_{tr}^{e} \right] = \int_{0}^{l} \mu \left[\psi_{fl} \right]^{T} \left[\psi_{fl} \right] ds, \quad \left[m_{ro}^{e} \right] = \frac{1}{2} \int_{0}^{l} \bar{I}_{P} \left[\psi_{ro} \right]^{T} \left[\psi_{ro} \right] ds$$

$$\left[\psi_{fl} \right] = \begin{bmatrix} \lfloor \psi_{fl} \rfloor_{x} \\ \lfloor \psi_{fl} \rfloor_{y} \end{bmatrix} \qquad \left[\psi_{ro} \right] = \begin{bmatrix} \lfloor \psi_{ro} \rfloor_{x} \\ \lfloor \psi_{ro} \rfloor_{y} \end{bmatrix}$$

$$\left[n^{e} \right] = \left[n_{a}^{e} \right] - \left[n_{b}^{e} \right]$$

$$\left[n_{a}^{e} \right] = \int_{0}^{l} \bar{I}_{P} \lfloor \psi_{ro} \rfloor_{x}^{T} \lfloor \psi_{ro} \rfloor_{y} ds \qquad \left[n_{b}^{e} \right] = \int_{0}^{l} \bar{I}_{P} \lfloor \psi_{ro} \rfloor_{y}^{T} \lfloor \psi_{ro} \rfloor_{x} ds$$

(10)

In Eqs. (6) and (7), the symbol{ }represents a column vector and $\lfloor \ \rfloor$ represents a row vector. Translational, flexural and rotational shape functions are denoted by ψ_{fl}, ψ_{ro} and ϕ_{to} for the Euler-Bernoulli beam. μ is the mass of the shaft per unit length, r is the shaft radius and $\bar{I}_{p}$ is the polar moment of inertia.

Substituting Eqs. (4) and (6) into the Lagrange's equation, the equations of motions for the assembled elements of the geared rotor structure will be obtained as follows:

$$[m^{s}]\{\ddot{q}^{s}\} + [g^{s}]\{\dot{q}^{s}\} + [k^{s}]\{q^{s}\} = \{f^{s}\} \tag{11}$$

where, $\{f^{s}\}$ is the force vector calculated by the virtual work principle[23]. The mass $[m^{s}]$, gyroscopic $[g^{s}]$ and stiffness $[k^{s}]$ matrices of the shaft are obtained by assembling the elements matrices with ten degrees of freedom.

3. Condition Monitoring

3.1. Model Updating

Model updating process for condition monitoring includes two parts: model tuning and damage identification. In the first part of the process, by using the measured vibration data from the undamaged state of a structure, the initial FE model is tuned to obtain an updated model in the undamaged state denoted as the intact model (undamaged model). Then the intact model is updated to obtain a calibrated model in the damaged state using the measured vibration data from the damaged state of the structure. Damaged parameters are identified by comparison of undamaged and damaged models. Modal characteristics of a structure are described by eigenvalue equations as:

$$([K] - \lambda_{i}[M])\{\phi_{i}\} = 0, \ i = 1 \ldots, n \tag{12}$$

where $[K]$ and $[M]$ are stiffness and mass matrices of the structure, respectively. λ_i is the ith eigenvalue of the system equal to the square of natural frequency, $\{\phi_i\}$ is the ith mode shape (eigenvector) of the intact structure and n is the number of degrees of freedom for the structure. The mode shapes are normalized with respect to the mass matrix.

Damage can cause changes in the stiffness matrix of a structure by an amount of $[\delta K]$. Change in the mass matrix due to the damage is neglected [24] . The variations in the stiffness matrix results in a change in the eigenvalue $\delta\lambda_i$ and also the corresponding eigenvector $\{\delta\phi_i\}$. Therefore, the eigenvalue equation of the damaged structure is given by:

$$([K]+[\delta K]-(\lambda_i+\delta\lambda_i)[M])(\{\phi_i\}+\{\delta\phi_i\})=0 \tag{13}$$

By pre-multiplying Eq. (10) by transpose of the mode shape vector $\{\phi_i\}^T$ and applying orthogonally condition, the following equation is obtained for variation of the squared natural frequency [25]:

$$\delta\lambda_i = \frac{(\{\phi_i\}^T[\delta K]\{\phi_i\}+\{\phi_i\}^T[\delta K]\{\delta\phi_i\})}{(1+\{\phi_i\}^T[M]\{\delta\phi_i\})} \tag{14}$$

Since the variation of each mode shape vector is orthogonal to the corresponding mode shape and due to the orthogonal property of the ith mode shape with respect to the rest of mode shapes, the term $\{\phi_i\}^T[M]\{\delta\phi_i\}$ vanishes. Measuring the mode shapes of experimental structures requires a complex sensor set up and also special sensors such as laser Doppler velocimeter (LDV). Hence, due to the complexity of the measurement and small amount of variations, all terms in Eq. (11) associated with the variations in the mode shapes have been neglected by many researchers 25. Therefore, the variation of the ith eigenvalue was evaluated by excluded mode shape (EMS) changes method as:

$$\delta\lambda_i = \{\phi_i\}_{1\times n}^T[\delta K]_{n\times n}\{\phi_i\}_{n\times 1} \tag{15}$$

The sensitivity equation is extracted from Eq. (12) as:

$$\{\delta\lambda\}_{n\times 1} = [S]_{n\times n}\{\delta p\}_{n\times 1} \tag{16}$$

Where the sensitivity matrix is shown by [S] and $\{\delta p\}$ illustrates the changes in each parameter. Also $\{\delta\lambda\}$ is the vector of eigenvalues. The number of eigenvalues is denoted by n. Solving sensitivity equations by the least square method results in the minimum parameters changes.

3.2. Improved Sensitivity Equation

Derivation of the eigenvalue equation Eq. (9), with respect to the tuning parameter is as follows:

$$([K]-\lambda_i[M])\{\phi_i'\}=-([K]-\lambda_i[M])'\{\phi_i\} \tag{17}$$

where $\{\phi_i\}'$ is the rate of changes of ith mode shape. The eigenvectors of the system introduce an orthogonal space vector that can be used to represent any vector of the same order by their linear combination[25].

$$\{\phi_i\}' \cong \sum_{j=1}^{n} \bar{\alpha}_{ij}\{\phi_j\} \tag{18}$$

where $\bar{\alpha}_{ij}$ is the participation factor of the jth mode shape used in the calculation of the rate of change of ith mode shape. By substituting Eq. (15) into Eq. (14), pre-multiplying by $\{\phi_k\}^T$ for $k \neq i$ and applying the orthogonal property of mode shapes with respect to the mass matrix:

$$\bar{\alpha}_{ik} = \frac{\{\phi_k\}^T([K]' - \lambda_i[M'])\{\phi_i\}}{(\lambda_i - \lambda_k)} \qquad k \neq i \tag{19}$$

where, $[K]'$ and $[M]'$ are the rate of changes of the stiffness and mass matrices, respectively. For $k = i$, derivation of the normalized mode equation $\{\phi_i\}^T[M]\{\phi_i\} = 1$, results in:

$$\{\phi_i^T\}'[M]\{\phi_i\} + \{\phi_i\}^T[M']\{\phi_i\} + \{\phi_i\}^T[M]\{\phi_i\}' = 0 \tag{20}$$

Substituting Eq. (15) into Eq. (17) and applying the orthogonal property yields:

$$\bar{\alpha}_{ii} = -\frac{\{\phi_i\}^T[M]'\{\phi_i\}}{2} \tag{21}$$

Using Eqs. (16) and (18), the rate of change of the ith mode shape can be calculated from the derivatives of stiffness and mass matrices, together with the eigenvalues and eigenvectors for all the modes.

Changes in the mode shapes of the system due to the damage can be evaluated using a first-order series as [25]:

$$\{\delta\phi_i\} \cong \sum_{j=1}^{n} \bar{\alpha}_{ij}\{\phi_j\}$$

$$\bar{\alpha}_{ij} = \frac{\{\phi_j\}^T[\delta K]\{\phi_i\}}{(\lambda_i - \lambda_j)}, j \neq i \quad and \quad \bar{\alpha}_{ii} = 0 \tag{22}$$

As mentioned before, any variations in the mass matrix were assumed to be negligible, therefore $\alpha_{ii} = 0$. Now, Eq. (11) can be rewritten to determine the changes of the natural frequencies (eigenvalues) by including the changes of mode shapes through Included Mode Shape (IMS) changes method as [25]:

$$\delta\lambda_i = \{\phi_i\}^T[\delta K]\{\phi_i\} + \{\phi_i\}^T[\delta K]\sum_{j=1}^{n}\frac{\{\phi_j\}^T[\delta K]\{\phi_i\}}{\lambda_i - \lambda_j}\{\phi_j\} \tag{23}$$

By using this algorithm to consider the mode shape changes in the damage detection process, the sensitivity of natural frequencies is characterized as a second-order element level function of the stiffness reduction. Therefore, because of the nonlinear dependency of the parameters in Eq. (19) the "fmincon" function in Matlab was used to determine the change of the stiffness.

3.3. Particle swarm optimization

Particle Swarm Optimization (PSO) method applies the concept of social interaction to problem-solving. In PSO, a swarm of n individuals communicates either directly or indirectly with one another search directions. Particles can be seen as simple agents that fly through the search space and record (and possibly communicate) the best solution that they have discovered. A particle (individual) movement is composed of three factors: (1) current position (location) of the particle in the search space, (2) location of the best solution found so far by the particle itself and (3) location of the best solution found so far by all the particles [20]. So the kinematic parameters of the particle can be stated as:

$$v_j^i = wv_j^i + c_1r_1(x_j^{i,best} - x_j^i) + (c_2r_2(x_j^{g,best} - x_j^i))$$
$$x_j^i = x_j^i + v_j^i$$

(24)

where x_j^i and v_j^i correspond to the values of the position and velocity vectors at iteration i for the particle j are generated at time t. $x_j^{i,best}$ is the location of the best solution found so far by the particle itself and $x_j^{g,best}$ The location of the best solution found so far by all the particles. As the algorithm is in progress, the position and the velocity of the particle are created by the algorithm mentioned in Eq. (20), where r_1, r_2 are the random coefficients in the interval of [0, 1] and c_1, c_2 are the learning coefficients.

The objective function of the optimization problem is defined as squares of the differences between the experimental and model natural frequencies:

$$Z = \sqrt{\sum_{i=1}^{4}(f_{A,i} - f_{E,i})^2}$$

(25)

where f_A and f_E represent the natural frequencies of the model and experimental setup, respectively. The summation is performed over four initial flexural natural frequencies.

4. Results and discussions

4.1. Numerical results

The rotor system consists of two shafts, four bearings and two gears as seen in Fig. (5). The driving shaft is connected to an AC motor by a coupling. The structure is also modeled numerically using FE method. Within the simulations, each shaft is divided into four beam elements with five nodes. Therefore, the FE model of the whole structure consists of 10 nodes and 8 elements. The shafts are made of steel with Young's modulus of $200GPa$ and the mass density of 7800 kg/m3. The gears are also made of aluminum with Young's modulus of $70GPa$ and the mass density of 2700 kg/m3. The two gears are simulated as two rigid disks with a concentrated mass located on nodes 3 and 5. Contact of the gears is modelled by employing

some springs with unknown gear translational (K_t) Fig. (3) and rotational (K_r) Fig. (4) contact stiffness matrices.
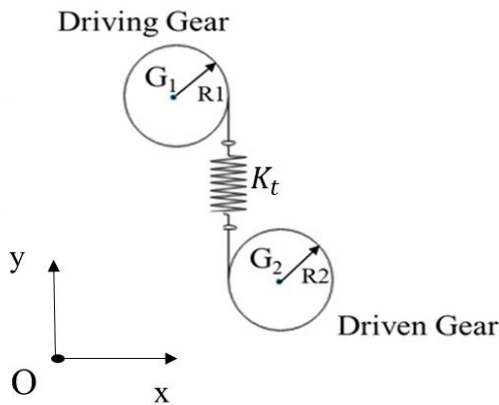
Fig. (3). Gear translational contact stiffness
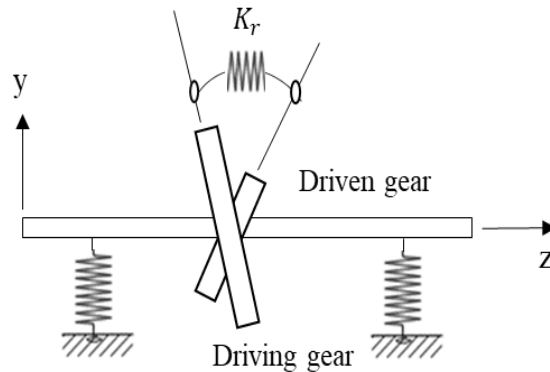
Fig. (4). Gear rotational contact stiffness

Also, bearings are modelled by springs with a known stiffness. Moreover, the mass, stiffness and gyroscopic matrices are extracted according to the principles of rotor dynamics as mentioned in section (2). The initial values of K_t and K_r are approximated to be 2×10^7 and 1.2×10^6 N/m, respectively. The FE model with these parameters is defined as the initial model. These values are to be updated within the model tuning process. The tuned models are called actual. By applying the coupled flexural and torsional vibration FE model of the rotor geared system, free vibration analysis is carried out and the modal characteristics are obtained by solving the eigenvalue problem. The first flexural four natural frequencies of the initial model are shown in Table (1).

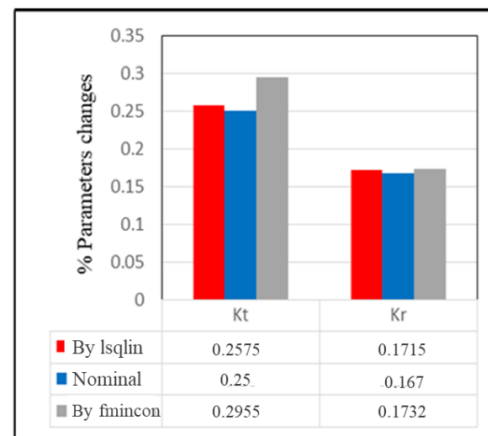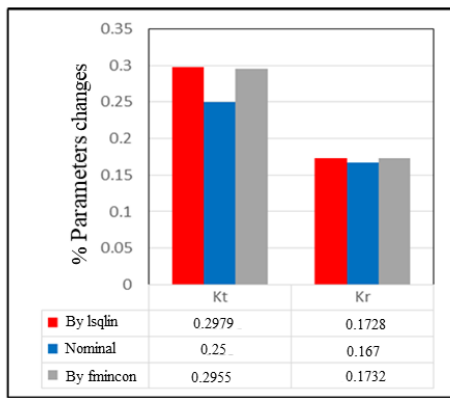## 4.2. Model verification of solving the sensitivity equation

To verify the accuracy of FE model and the solution of the sensitivity equation, the initial and actual models are defined. The actual model is obtained by the sensitivity analysis on two parameters K_t and K_r. Therefore, the nominal value changes of the K_t and K_r are known for the actual model in comparison to the initial model. To obtain the values of parameters changes, the sensitivity equation must be solved for each parameter. The natural frequencies of the actual model are shown in Table (2). The amount of nominal and predicted changes of the parameters for 1 iteration of solving the sensitivity equation by least square method (lsqlin) and "fmincon" function in Matlab are compared in Fig. (5). In the least square method, the term of mode shape changes is omitted (EMS) and in "fmincon" method it is assumed to be a linear combination of eigenvectors for all modes (IMS).

Table 1. Natural frequencies of the initial model

Mode No.	Natural Frequency (Hz) (Analytical)
1	34.33
2	40.9
3	48.25
4	56.2

Table 2. Natural frequencies of the actual model

Mode No.	Natural Frequency (Hz) (Analytical)
1	32.15
2	40.67
3	48.13
4	56.1

Fig. (5). Nominal and predicted changes of the parameters for 1 iteration of solving the sensitivity equation

Fig. (6). The actual model and predicted changes of the parameters for 50 iterations solving the sensitivity equation

Table (3) shows the actual model and predicted values of updated parameters for 1 iteration of solving the sensitivity equation.

Table 3. The actual model and predicted values

	Actual model value (N/m)	Predicted value by lsqlin (N/m)	Predicted value by fmincon (N/m)
K_t	1.5×10^7	1.4041×10^7	1.4090×10^7
K_r	1×10^6	9.9263×10^5	9.9216×10^5

As it can be seen, the results of predicted values for 1 iteration solving the sensitivity equation is not accurate. Therefore, the number of iterations are increased to 50. The amount of nominal and predicted changes of the parameters are shown in Fig. (6). Table (4) shows the actual model and predicted values of updated parameters for 50 iterations solving the sensitivity equation by two abovementioned methods.

Table 4. Actual model and predicted values

|	Actual model value (N/m)	Predicted value by lsqlin (N/m)	Predicted value by fmincon (N/m)
K_t	1.5×10^7	1.4849×10^7	1.4090×10^7
K_r	1×10^6	9.9414×10^5	9.9216×10^5

As seen in Table (3) and Table (4), the results of the "fmincon" function is not as accurate as of the least square method. Therefore, the least square method with 50 iterations was used to predict the damage. Besides, natural frequencies of the experimental setup are extracted. In the following, the natural frequencies of the model are matched with the natural frequencies obtained from the experiment. Then, the intensity of the damage is obtained from the differences in the natural frequencies in the healthy and damaged modes.

4.3. Experimental Results

To verify the accuracy of the method in detecting damages in the presence of measured noise and modelling error, an experimental setup is used as illustrated in Fig. (7). In the experimental setup, four piezoelectric accelerometers were mounted on four bearings in the rectangle corners in X and Z directions to acquire time-domain data. After importing data into ARTeMIS software and applying the stochastic subspace identification (SSI) method, the flexural natural frequencies are obtained for the intact structure. Power spectral density (PSD) data obtained from ARTeMIS in the healthy condition is shown in Fig. (8). Also, the resultant flexural natural frequencies in healthy mode are shown in Table (5).
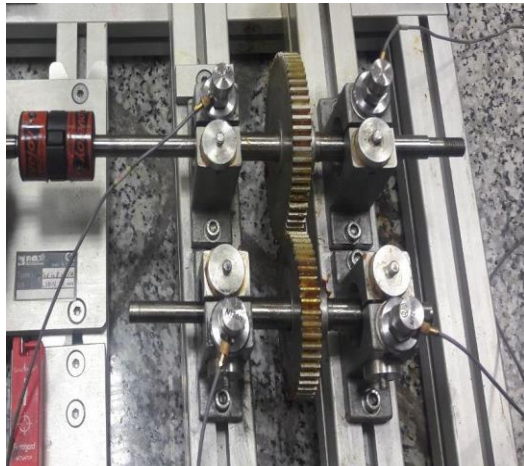
Fig. (7). Experimental setup
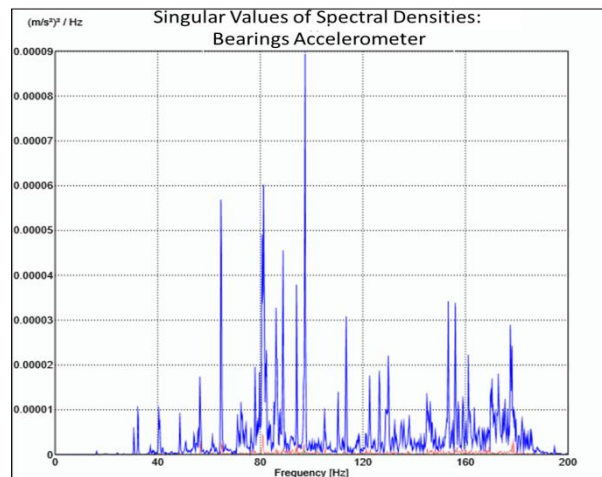
Fig. (8). PSD from ARteMIS in healthy condition

The modal characteristics of the initial model are updated to the modal characteristics of the experimental setup. The value of each parameter changes is shown in Fig. (9). Table (6) shows the predicted values of updated parameters.

Table 5. Natural frequencies of the experimental setup in healthy mode

	Natural Frequency (Hz)
Mode No.	(Experimental)
1	32.084
2	40.67
3	48.151
4	56.207

Table 6. Predicted values of updated parameters

	Initial model value (N/m)	Predicted value (N/m)
K_t	2×10^7	1.4849×10^7
K_r	1.2×10^6	9.9414×10^5

Differences between the measured and initial model natural frequencies are due to the modelling errors and differences in the tuning parameters between the initial model and the experimental setup. In this stage of model updating (model tuning) the unknown variables experience a wide range of variations.

|	Kt	Kr
■ Predicted	0.262	0.161
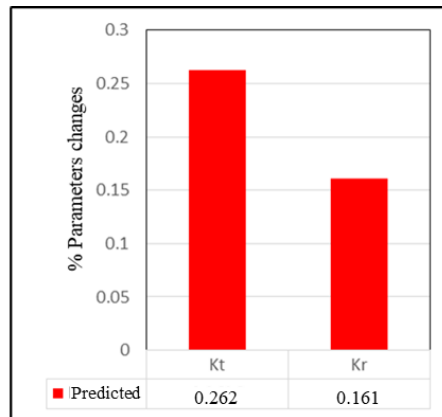
Fig. (9). Predicted changes of updated parameters

In this paper, damage detection processes are done by model updating method solving the sensitivity equation for 50 iterations and PSO method. PSO is applied for a population of 40, 20 iterations, and two tuning parameters. Personal and social learning coefficients and inertia coefficients are 2, 1.7 and 0.7, respectively. The results of damage intensity are calculated by two methods.

4.4. Damage detection

After obtaining the updated model of the structure, different types of damages are introduced in one of the gears of the experimental setup to demonstrate different damage regimes in the geared rotor system. Then flexural natural frequencies of the defected structure are obtained by ARTeMIS. Therefore, in this part, the parameters in the model are updated to match the natural frequencies of the model with that of the damaged setup.

4.4.1. Tooth breakage fault

The tooth breakage fault is shown in Fig. (10). The flexural natural frequencies of the system in the presence of tooth breakage fault and the percent of frequency changes (PFCs) concerning the healthy mode are listed in Table (7). The parameter changes by model updating method and PSO are shown in Fig. (11) and Fig. (12). The predicted values of K_t and K_r by two methods are shown in Table (8).
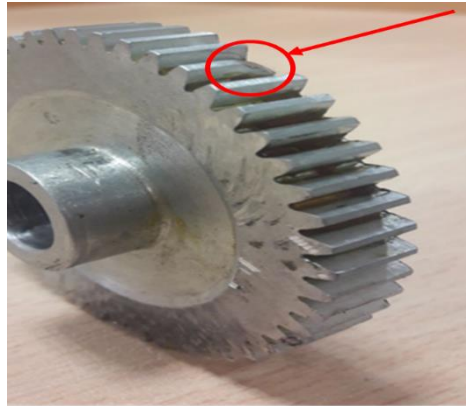
Fig. (10). Tooth breakage fault
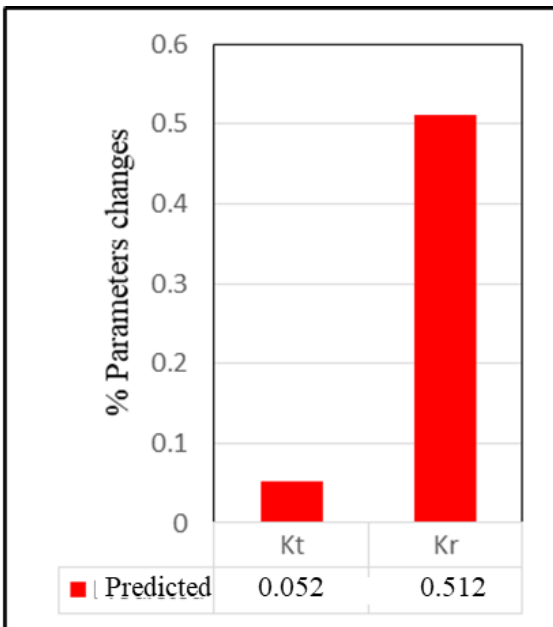
Fig. (11). Predicted values of damaged parameters by model updating
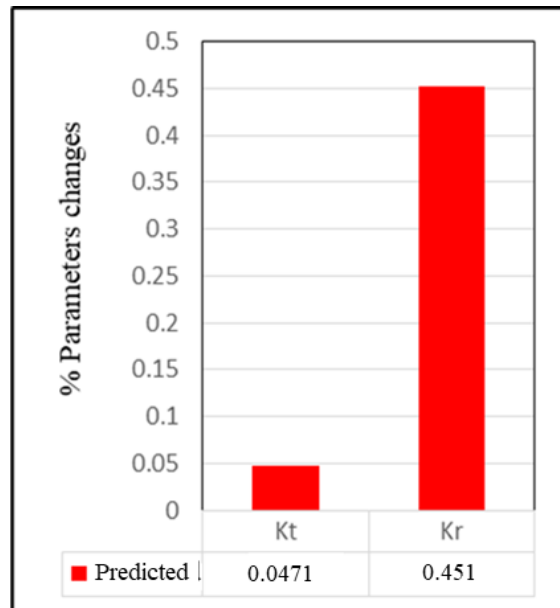
Fig. (12). Predicted values of damaged parameters by PSO

Table 7. Natural frequencies of tooth breakage

Mode No.	Natural Frequency (Hz) (Damaged structure)	PFC*
1	31.75	-1.04
2	40.38	-0.71
3	47.26	-1.85
4	54.64	-2.78

* Percent of Frequency Changes

Table 8. Predicted values of K_t and K_r

	Model updating	PSO
K_t (N/m)	1.3977×10^7	1.4177×10^7
K_r (N/m)	4.9146×10^5	5.5109×10^5

4.4.1. Tooth crack fault

The tooth crack fault is shown in Fig. (13). The flexural natural frequencies of the system with a cracked tooth and the PFCs regardingthe healthy mode are shown in Table (9). Changes in the parameters by model updating method and PSO are shown in Fig. (14) and Fig. (15). Also, the predicted values of K_t and K_r by two methods are listed in Table (10).

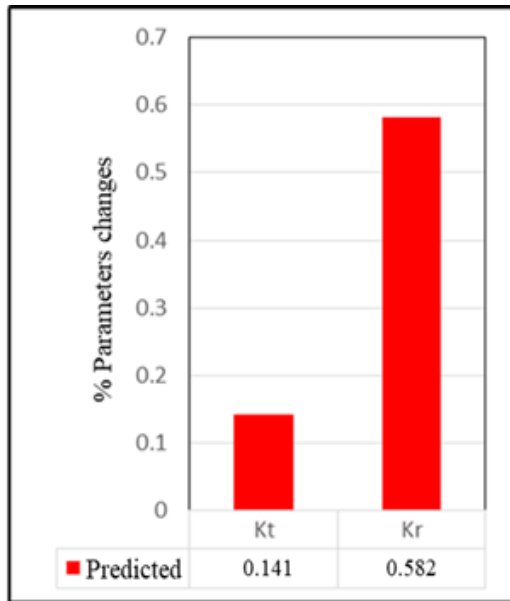**Table 9.** Natural frequencies of tooth crack

Mode No.	Natural Frequency (Hz) (Damaged structure)	PFC
1	30.86	-3.81
2	40.43	-0.59
3	46.88	-2.64
4	55.27	-1.67

Table 10. Predicted values of K_t and K_r

	Model updating	PSO
K_t (N/m)	1.2677×10^7	1.2891×10^7
K_r (N/m)	4.2096×10^5	5.1159×10^5

Fig. (13). Tooth crack fault

Fig. (14). Predicted values of damaged parameters by model updating
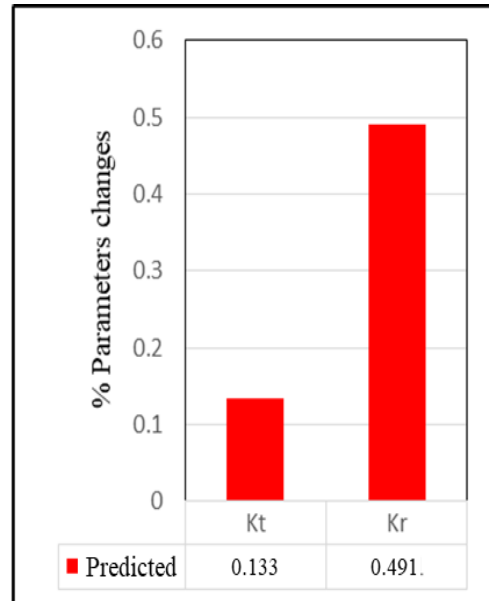
Fig. (15). Predicted values of damaged parameters by PSO

4.4.2. Missing tooth fault

The missing tooth fault is shown in Fig. (16). Also, corresponding flexural natural frequencies of the system for this situation and PFCs with respect to the healthy mode are shown in Table (11). The variations of parameters by model updating and PSO methods are shown in Fig. (17) and Fig. (18). The predicted values of K_t and K_r by two methods are listed in Table (12).


Fig. (16). Missing tooth fault

Table 11. Natural frequencies of the missing tooth

Mode No.	Natural Frequency (Hz) (Damaged structure)	PFC
1	30.47	-5.03
2	40.23	-1.08
3	46.48	-3.47
4	54.9	-2.32

Table 12. Predicted values of K_t and K_r

	Model updating	PSO
K_t (N/m)	1.2054×10^7	1.2255×10^7
K_r (N/m)	2.3968×10^5	3.1630×10^5

To get an insight into the applicability of the two condition monitoring methods, namely model updating, and PSO methods, the results are compared for three types of damages created on the gears. The stiffness changes indicate the percent of reduced contact stiffness for damaged gears.
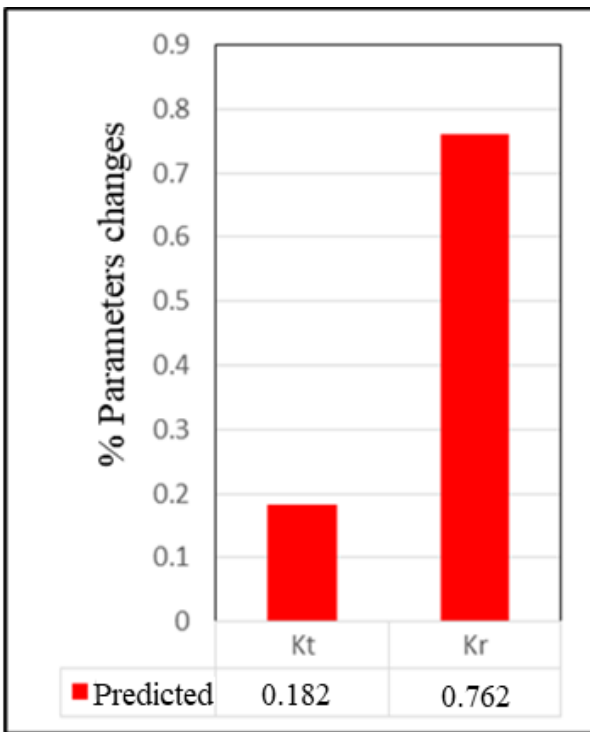
Fig. (17). Predicted values of damaged parameters by model updating
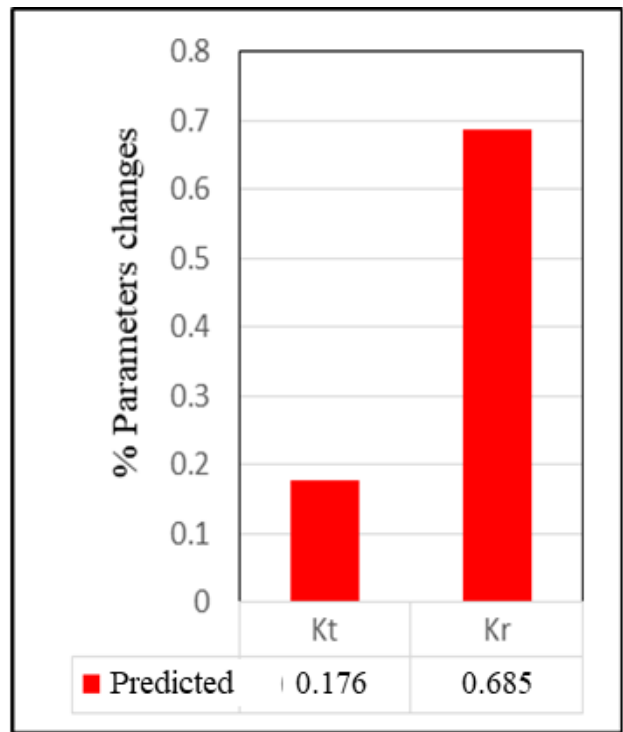
Fig. (18). Predicted values of damaged parameters by PSO

The results of two methods are acceptable, although PSO predicts the changes in contact stiffness more precisely than the updating method because of the approximated terms in the model updating method. The intensity and type of damage are recognizable by Table (13).

Results show a decrease in the contact stiffness of the gear due to the increase of the intensity of damage and its effects on system stability when the shaft rotational speed increases. The accuracy of the applied method is dependent on the measured flexural natural frequencies and efficiency of the optimization algorithm. In this study, the first flexural four natural frequencies are chosen and the results of two applied methods are approximately similar to each other that shows the accuracy of two methods.

Table 13. Intensity and type of damage by model updating and PSO

Type of fault	Condition method	Translational contact stiffness changes	Rotational contact stiffness changes
Tooth breakage	Updating	0.052	0.512
	Optimization	0.047	0.451
Tooth crack	Updating	0.141	0.582
	Optimization	0.133	0.491
Missing tooth	Updating	0.182	0.762
	Optimization	0.176	0.683

5. Conclusion

This paper presented finite element model updating and particle swarm optimization (PSO) methods for damage detection in a geared rotor system based on measured flexural natural frequencies. Numerical results showed that the accuracy of a frequency-based method is dependent on the number of the measured natural frequencies and severity of the damage. Therefore, based on the literature review, four flexural natural frequencies were chosen. At first, the verification of the model was done by defining the actual model of the structure with known parameters. In the following, to obtain the updated model of the structure, the flexural natural frequencies of the model were matched the measured data. Then, a damage detection process was proposed to detect the changes in the system parameters. Model updating method for 50 iterations of solving the sensitivity equation and particle swarm optimization was applied. Although the results of two methods were reliable, the optimization method was able to predict the parameters changes more accurately than the model updating method because of the neglected terms in the sensitivity equations. For the Fault of tooth cracks, the optimization

method predicts the reduced translational and rotational contact stiffness changes as 0.133 and 0.491, compared to the model updating method which predicts the damage as 0.141 and 0.582.

References

[1] O.D. Mohammed, M. Rantatalo, J.O. Aidanpää, Dynamic modelling of a one-stage spur gear system and vibration-based tooth crack detection analysis, Mechanical Systems and Signal Processing, 54 (2015) 293-305.

[2] Z. Feng, M.J. Zuo, F. Chu, Application of regularization dimension to gear damage assessment, Mechanical Systems and Signal Processing, 24 (2010) 1081-1098.

[3] Z. Feng, M.J. Zuo, Fault diagnosis of planetary gearboxes via torsional vibration signal analysis, Mechanical Systems and Signal Processing, 36 (2013) 401-421.

[4] W. Bartelmus, Object and operation supported maintenance for mining equipment, Mining Science, 21 (2014) 7--21.

[5] W. Bartelmus, R. Zimroz, Vibration spectra characteristic frequencies for condition monitoring of mining machinery compound and complex gearboxes, Mining Science, 133 (2011) 17.

[6] M. Inalpolat, A. Kahraman, A theoretical and experimental investigation of modulation sidebands of planetary gear sets, Journal of sound and vibration, 323 (2009) 677-696.

[7] Z. Feng, M.J. Zuo, Vibration signal models for fault diagnosis of planetary gearboxes, Journal of Sound and Vibration, 331 (2012) 4919-4939.

[8] R. Patrick, A.l. Ferri, G. Vachtsevanos, Effect of planetary gear carrier-plate cracks on vibration spectrum, Journal of vibration and acoustics, 134 (2012).

[9] A. Parey, N. Tandon, Spur gear dynamic models including defects: A review, The Shock and Vibration Digest, 35 (2003) 465-478.

[10] W. Bartelmus, Supporting diagnostic inference by mathematical modelling from one-stage to planetary gearbox systems, Diagnostyka, 30 (2004) 31-38.

[11] Y. Lei, J. Lin, M.J. Zuo, Z. He, Condition monitoring and fault diagnosis of planetary gearboxes: A review, Measurement, 48 (2014) 292-305.

[12] H. Ma, J. Zeng, R. Feng, X.u. Pang, Q. Wang, B. Wen, Review on dynamics of cracked gear systems, Engineering Failure Analysis, 55 (2015) 224-245.

[13] A.S. Lee, J.W. Ha, D.-H. Choi, Coupled lateral and torsional vibration characteristics of a speed increasing geared rotor-bearing system, Journal of Sound and Vibration, 263 (2003) 725-742.

[14] M.l. Friswell, J.E. Mottershead, Finite element model updating in structural dynamics, Springer Science & Business Media, 2013.

[15] T. Marwala, Finite element model updating using computational intelligence techniques: applications to structural dynamics, Springer Science & Business Media, 2010.

[16] E. Simoen, G. De Roeck, G. Lombaert, Dealing with uncertainty in model updating for damage assessment: A review, Mechanical Systems and Signal Processing, 56 (2015) 123-149.

[17] A. Teughels, G. De Roeck, Damage detection and parameter identification by finite element model updating, Revue européenne de génie civil, 9 (2005) 109-158.

[18] J.E. Mottershead, M. Link, M.I. Friswell, The sensitivity method in finite element model updating: a tutorial, Mechanical systems and signal processing, 25 (2011) 2275-2296.

[19] J. Kennedy, R.C. Eberhart, Particle swarm optimizationProceedings of IEEE International Conference on Neural Networks, Perth, WA, Australia), Vol. 4, pp 1942–1948, IEEE Service Center, Piscataway, NJ, (1995).

[20] R. Poli, Analysis of the publications on the applications of particle swarm optimisation, Journal of Artificial Evolution and Applications, 2008 (2008).

[21] S.-W. Lin, K.-C. Ying, S.-C. Chen, Z.-J. Lee, Particle swarm optimization for parameter determination and feature selection of support vector machines, Expert systems with applications, 35 (2008) 1817-1824.

[22] Y. Ishida, T. Yamamoto, Linear and nonlinear rotordynamics, Wiley Online Library, 2012.

[23] Q. Han, J. Zhao, F. Chu, Dynamic analysis of a geared rotor system considering a slant crack on the shaft, Journal of Sound and Vibration, 331 (2012) 5803-5823.

[24] A. Esfandiari, F. Bakhtiari-Nejad, A. Rahai, Theoretical and experimental structural damage diagnosis method using natural frequencies through an improved sensitivity equation, International Journal of Mechanical Sciences, 70 (2013) 79-89.

[25] S. Hassiotis, G.D. Jeong, Identification of stiffness reductions using natural frequencies, Journal of engineering mechanics, 121 (1995) 1106-1113.